Supporting Information

Organic cathode materials Oligomerized Imide and Thioimide via H-transfer Mechanism for High Capacity Lithium ion Batteries

Xing-Chao Tu, [a,b‡] Zhenzhen Wu, [c‡] Xin Geng,[b] Lu-Lu Qu, [b*] Hong-Mei Sun, [a*] Chao Lai,[b] Dong-Sheng Li,[d] and Shanqing Zhang [c*]

[a] College of Chemistry, Chemical Engineering and Materials Science, Soochow University, Suzhou 215123, China

[b] School of Chemistry and Materials Science, Jiangsu Normal University, Xuzhou, Jiangsu 221116

[c] Centre for Clean Environment and Energy, School of Environment and Science, Gold Coast Campus, Griffith University, Southport, QLD, 4222, Australia.

[d] College of Materials and Chemical Engineering, Key Laboratory of Inorganic Nonmetallic Crystalline and Energy Conversion Materials, China Three Gorges University, Yichang, 443002, China

[‡] X. C. Tu and Z. Z. Wu are co-first authors who contributed equally to this work.

Email: s.zhang@griffith.edu.au, laichao@jsnu.edu.cn

Experimental Procedures

Raw Materials. Cyanuric acid (CA, chemical purity ≥99.5%), trithiocyanuric acid (TTCA, chemical purity ≥99.5%), and other raw materials were purchased from Shanghai Bidepharm Tech. Inc. ^{1}H and ^{13}C NMR spectra of all the organic materials are given in **Fig. S13.**

The synthesis of CA or TTCA in CMK-3. In the synthesis of the composite of CMK-3 and organic materials (CA and TTCA), 50 mg of the organic materials were dissolved in 5mL ethanol, added 200 mg CMK-3. The resultant mixture was subject to stirring for 20 mins and being dried in a vacuum oven for overnight at 60 °C.

Characterization. The discharged TTCA (or CA) electrode was firstly ultrasonically dissolved in DMSO-d_6. After filtration, the clear liquor was collected and subject to ^{1}H NMR (^{13}C NMR) analysis by Bruker DPX 400 MHz spectrometer with chemical shift (δ) given in ppm relative to TMS as an internal standard [(s = singlet, d = doublet, t = triplet, m = multiplet), coupling constant (Hz)]. Fourier transform infrared spectroscopy (Bruker Tensor 27) measurement was carried out in dry KBr to confirm the structures of all active materials. The morphologies of organic electrodes were observed by field-emission scanning electron microscopy (SEM, JEOL M-2800) under an accelerating voltage of 200 kV and transmission electron microscopy (TEM, Hitachi SU-8010) under an accelerating voltage of 25 kV. Ex-situ surface-enhanced Raman scattering (SERS) spectra were collected from a portable Raman spectrometer (BWS415, BWTEK Inc., U.S.A) with an excitation wavelength of 785 nm, an integration time of 5 s, and a laser power of 4 mW. Distributions of valence on surfaces of the organic cathodes were characterized by X-ray photoelectron spectroscopy (XPS, and Themo Scientific ESCALAB 250Xi system).

Theoretical calculations. Density theory functional calculations (DFT) were performed by using B3LYP hybrid density functional theory with 6-31G* basis sets implemented in Gaussian 03 software package. All the geometric structures were fully optimized under standard convergence criteria. The optimized structures were confirmed to be true minima by analytical

vibrational frequency calculations.[1] On the basis of the optimized structures, the binding energies were calculated as the difference between the energies of the complexes and the summed energies of all individuals. we simulate the electrochemical process by using the Li^+ ion and e^- to replace the lithium atom in our calculation, *i.e.,* TTCA+Li^++e^- →TTCALi, where the energy of Li^++e^- is treated as the energy of lithium atom. Transition states of proton transfer reactions were searched by the QST2 algorithm, further validated by vibration analysis, which displayed that only one imaginary frequency response the target reactions. IRC scans started from the transition states were finished by the LQA algorithm for confirming the reaction path of the proton transfer. To obtain the energy levels of CA and TTCA with respect to the vacuum level, periodic calculations were performed within the framework of DFT implemented in the Vienna ab initio simulation package (VASP).[2-4] The generalized gradient approximation with the functional was described by the Perdew-Burke-Ernzerhof type (PBE).[5] The projector-augmented wave (PAW) method[6] was applied to describe the wavefunctions in the core regions, while the valence wavefunctions were expanded as linear combination of plane-waves with a cutoff energy of 400 eV. The total energy was converged to 10-5 eV in the geometry optimizations, and the Hellmann–Feynman force on each relaxed atom was less than 0.02 eV/Å. The CA and TTCA molecules were placed in a big box of 15*15*20 Å.

Electrochemical Measurements. CA and TTCA were first mixed with CMK-3, respectively, with a mass ratio of 3:7 to fabricate a homogeneous composite. The electrodes were fabricated by mixing composites, conductive carbon black (Super-P), and the binder polytetrafluoroethylene (PVDF) at a mass ratio of 7:2:1. After coating on aluminum foil, the resultant electrodes were cut into discs with a diameter of 8 mm and a loading of 1.0 mg cm^{-2}. Lithium foil was used as the counter and reference electrodes. The applied electrolyte is 1.0 M Bis(trifluoromethane)sulfonimide lithium (LiTFSI) salt dissolved in the mixing solvent of 1,2-dimethoxyethane (DME) and 1,3-dioxolane (DOL) with a volume ratio of 1:1. Galvanostatic charge/discharge measurements were conducted on a LAND-CT2001A battery test instrument

(Wuhan, China), and cyclic voltammetry (CV) measurements were tested using CHI electrochemical workstation (Shanghai Chenhua Instrument, Inc) at room temperature.

Results and Discussion

General

Cyanuric acid (**CA**). White solid, mp > 300 °C; ^{1}H NMR (400 MHz, DMSO-d_6) δ 11.15 (s, 3H); ^{13}C NMR (100 MHz, DMSO-d_6) δ 150.4 (s); IR (KBr, v, cm^{-1}) 3025, 2780, 1779, 1753, 1720, 1590, 1466, 1397, 1058, 771, 753, 690, 535.

Trithiocyanuric acid (**TTCA**). Light green-yellow solid, mp > 300 °C; ^{1}H NMR (400 MHz, DMSO-d_6) δ 13.68 (s, 3H); ^{13}C NMR (100 MHz, DMSO-d_6) δ 172.3 (s); IR (KBr, v, cm^{-1}) 3135, 3040, 2907, 1577, 1523, 1361, 1297, 1258, 1119, 747, 666, 175, 457.

The mixture of addition agents including PVDF, NMP, LiTFSI, DME and DOL. ^{1}H NMR (400 MHz, DMSO-d_6) δ 4.78 (s), 3.78 (s), 3.43 (s), 3.31 (t, J = 7.2 Hz), 3.24 (s), 2.70 (s), 2.55 – 2.47 (m), 2.18 (t, J = 8.0 Hz), 1.91 (dt, J = 15.6, 7.4 Hz).

The calculation of experimental lithium ions transfer number.[7] The experimental electron transfer number (n) in the charge/discharge process can be calculated by the following equations:

$$n = \frac{Cexp * Mw}{F}$$

Where $C_{exp.}$ is the experimental specific capacity, Mw is the molecular weight and F is the Faraday constant with the value of 26801.

Type I (n/p) doping reaction

Radical polymer
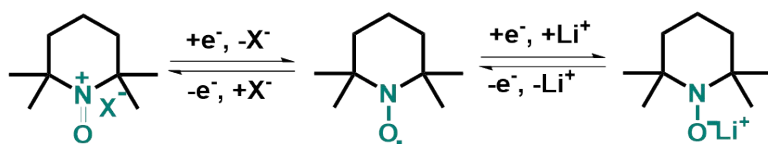
Type II The cleavage/regeneration of single bond reaction

S-S bond

$$R-S-S-R \underset{-2e^-, -2Li^+}{\overset{+2e^-, +2Li^+}{\rightleftharpoons}} 2R-SLi$$
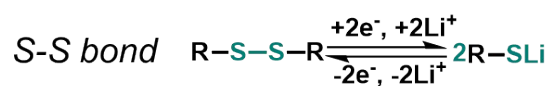
Type III The addition of double bond reaction

N=N bond

C=O bond

C=N bond

Organic salt
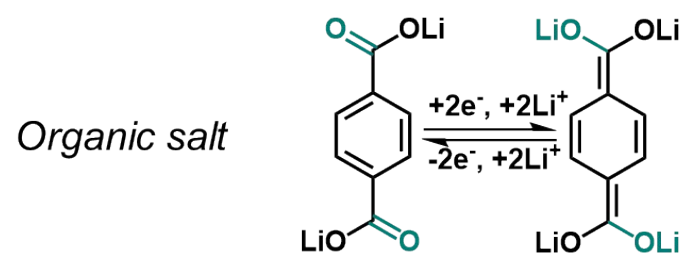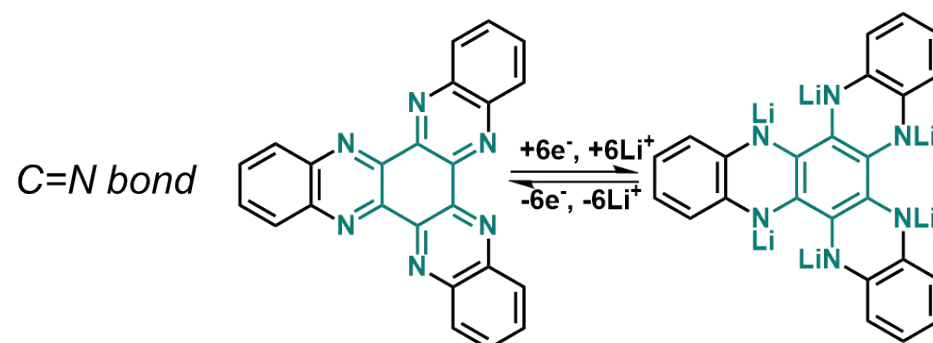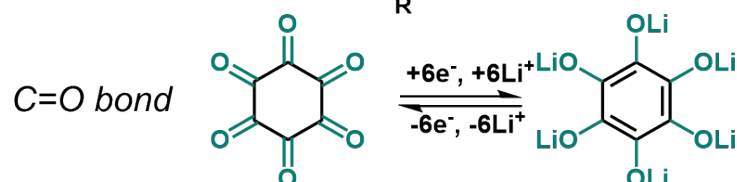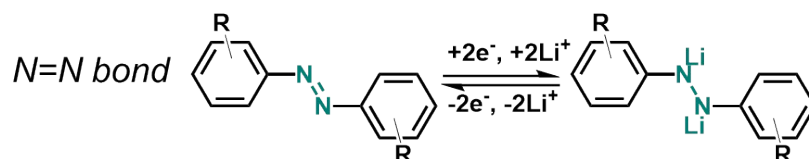
Scheme S1. The conventional chemistry reaction of organic electrode materials for lithium ions storage.
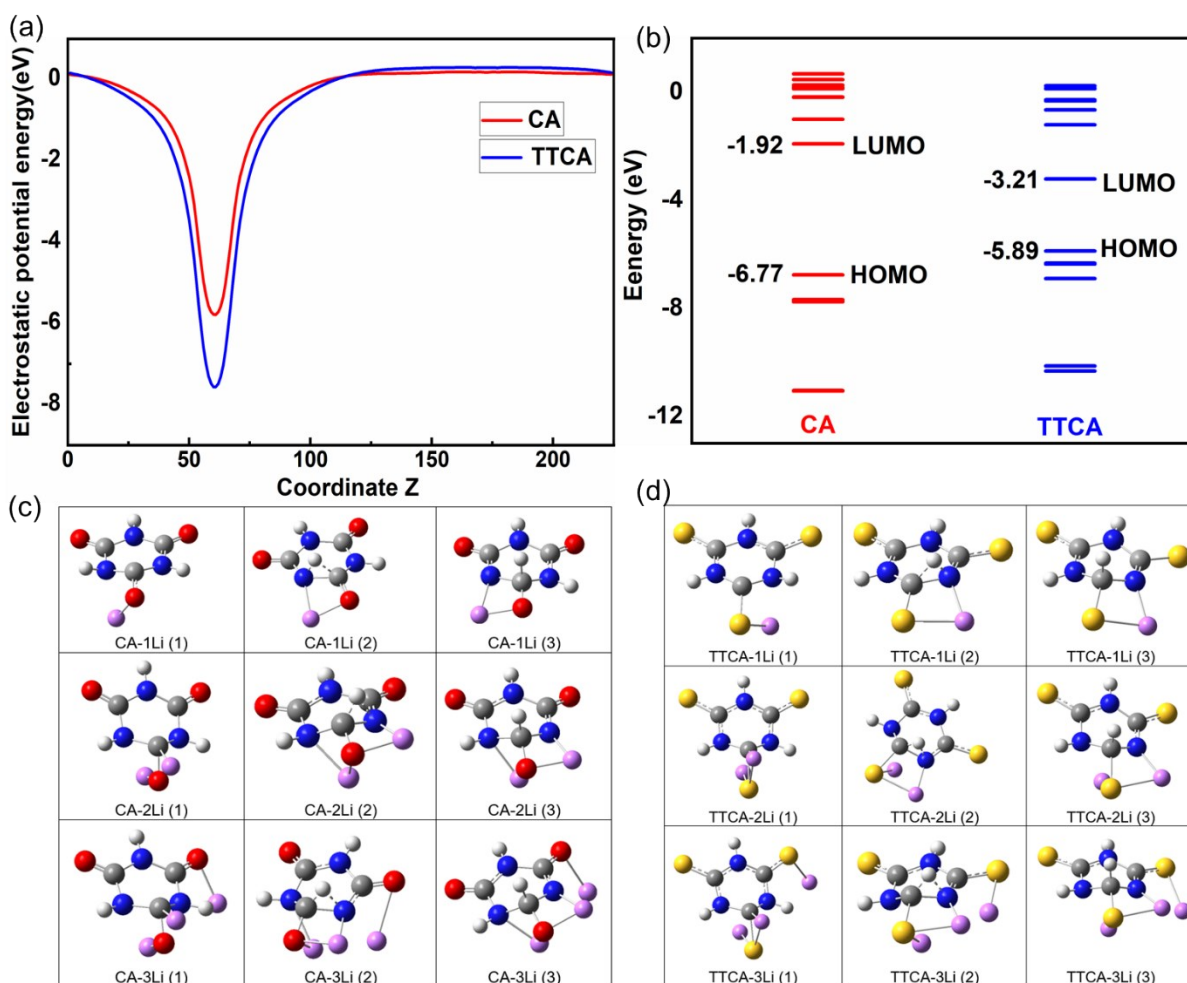
Figure S1. a-b Calculated electrostatic potential energies (a) and energy levels (b) of CA and TTCA with respected to vacuum levels. c-d The optimized molecular structures of lithiated CA (c) and TTCA (d) with 1-3 lithium atoms, where the red, blue, grey, white, yellow and pink balls represent oxygen, nitrogen, carbon, hydrogen, sulfur and lithium atoms, respectively.
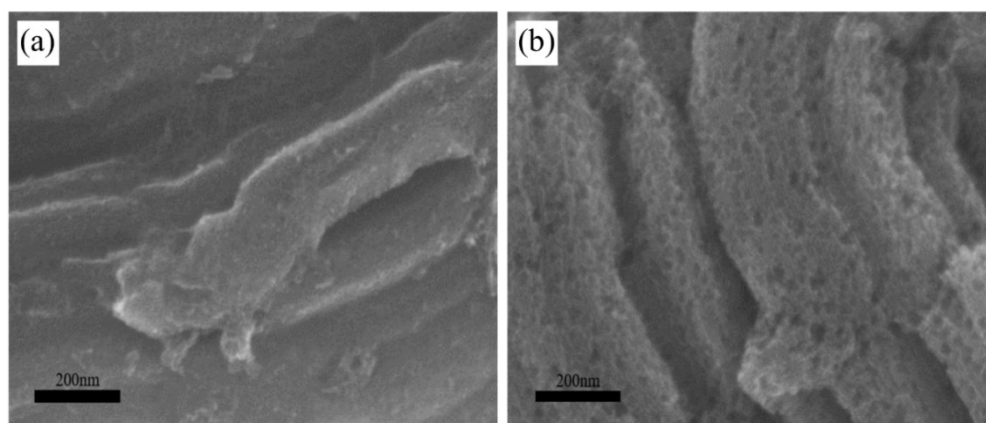
Figure S2. SEM images at high magnification of oligoimides and oligothioimides that combined with CMK-3. **(a)** CA and **(b)** TTCA.
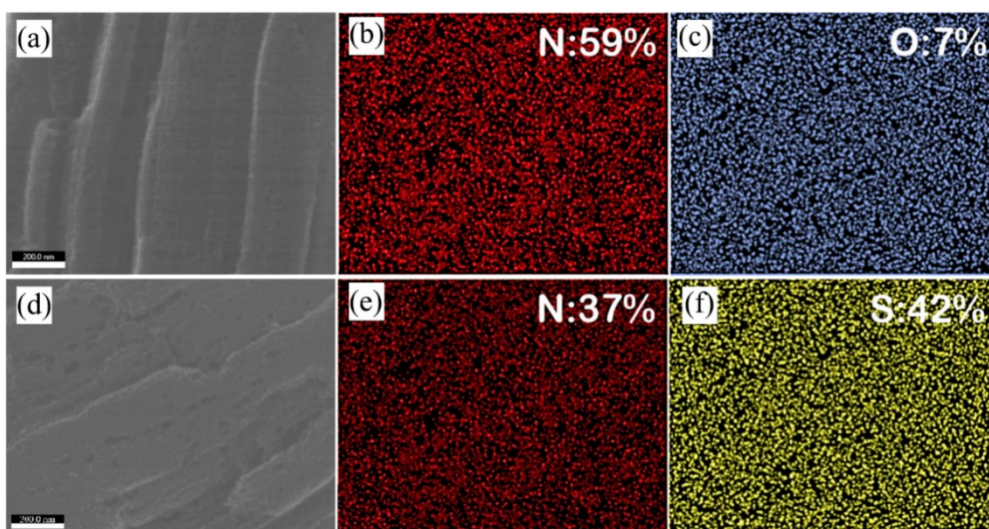
Figure S3. SEM and TEM of N and O images at high magnification for oligoimides and oligothioimides combined with CMK-3. **(a, b, c)** CA, **(d, e, f)** TTCA.
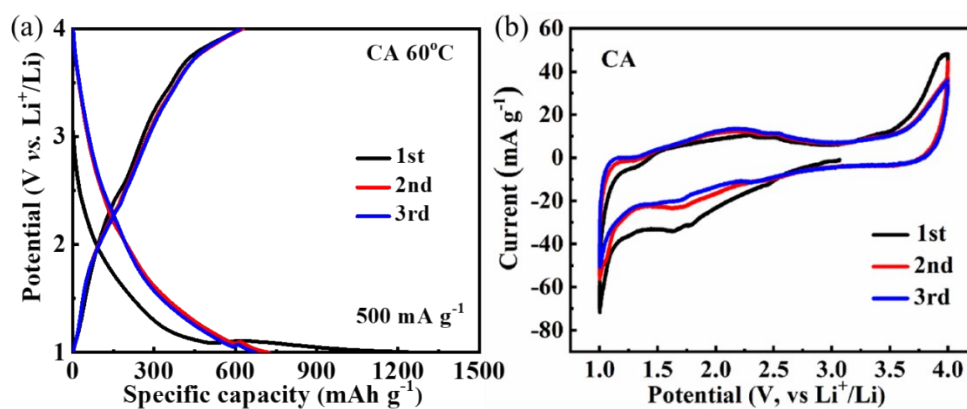
Figure S4. (a) Charge-discharge curves of the first three cycles of CA at 60 °C at 500 mA g^{-1}. (b) Cyclic voltammetry curves of CA at room temperature.
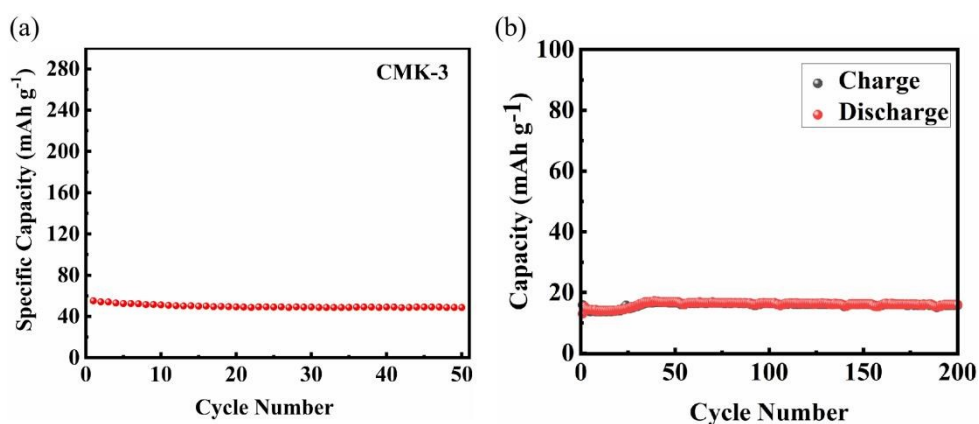
Figure S5. Long-term cycling performance of (a) CMK-3 and (b) surper P under the current density of 500 mA g^{-1}.

The discharge capacity of super P are investigated, and the results are given in Fig. S5. As shown, the capacity of super P is below 18 mAh g^{-1} and which is very low compared with the CA and TTCA capacity. This further confirms that the capacity of electrode is mainly generated from CA and TTCA.
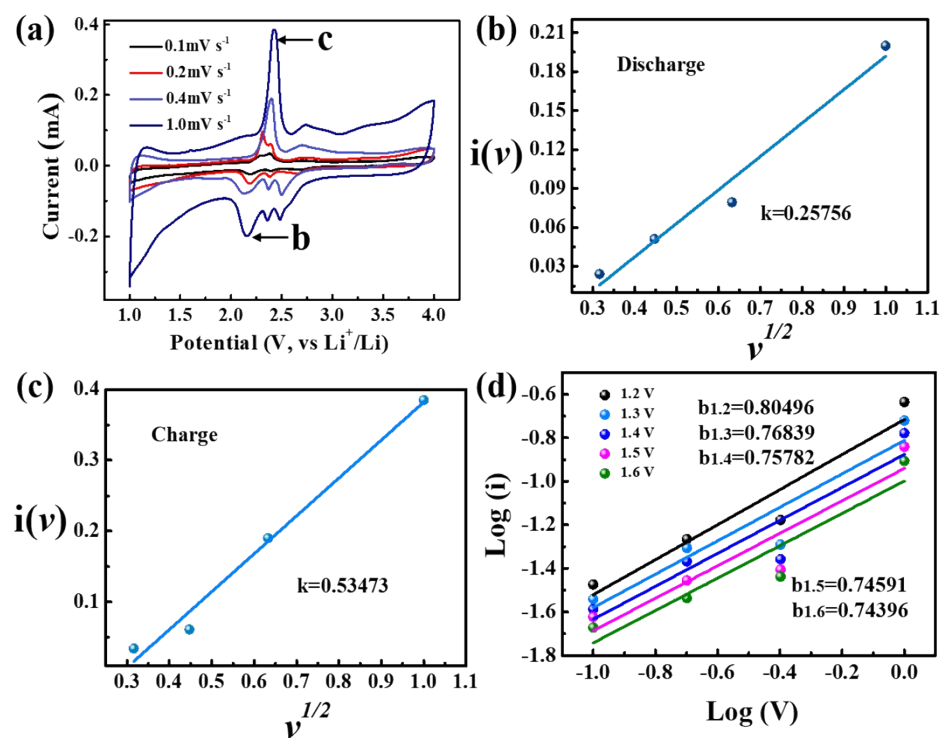
Figure S6. (a) Cyclic voltammetry curves of TTCA under different scan rates. (b) Calculation of the k value of TTCA discharge process. (c) Analysis of the k value of TTCA charge process. (d) Calculation of the b values of TTCA cathode.
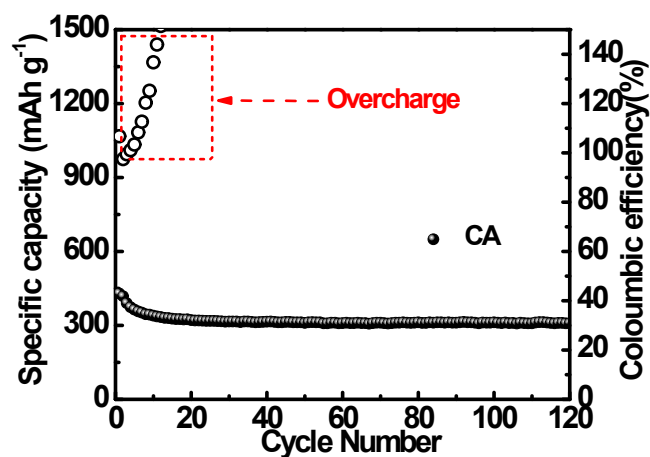
Figure S7. Cycling performance of CA-based organic electrodes at a currents of 2000 mA g^{-1}.

8
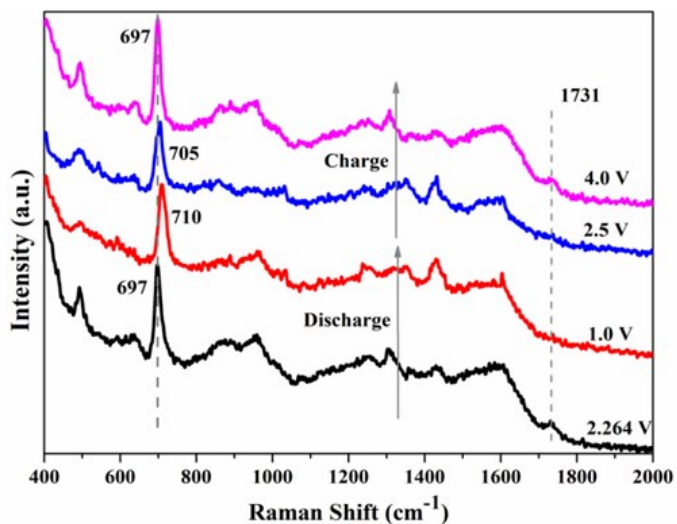
Fig. S8. Raman spectra of CA cathode in rechargeable Li batteries. The signals are collected at 2.264 V (black curves) and 1.0 V (red curves) in the discharge process, and 2.5 V (blue curves) and 4.0 V (rose red) during charge process.
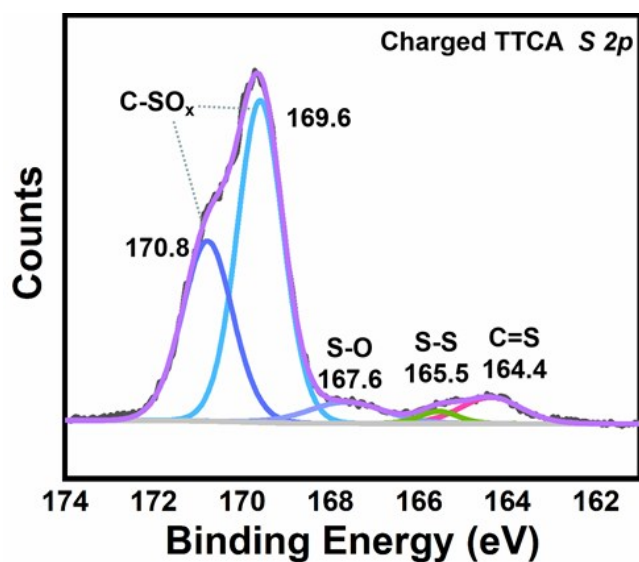
Figure S9. S 2p XPS spectra of charged and discharged TTCA cathode.
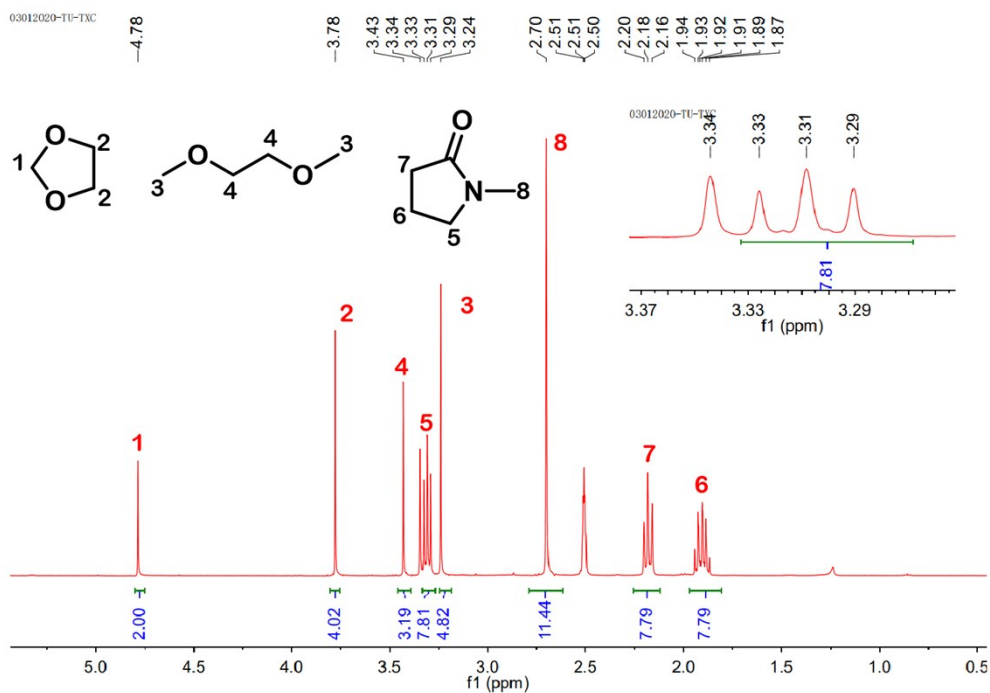
Figure S10. Detail ^{1}H NMR information of addition agents. Eight kinds of H were found and attributed to corresponding molecules.

To further demarcate attributions of other characteristic peaks of the black curve in Fig. 4g, addition agents including, polyvinylidene fluoride (PVDF, used as adhesive), N-methylpyrrolidin-2-one (NMP, used as the solvent of adhesive), solution of lithium bis((trifluoromethyl)sulfonyl)amide (LiTFSI) in mixture solvent of 1,2-dimethoxyethane and 1,3-dioxolane (DME & DOL, mixed in a ratio of 1:1, used as electrolyte), are mixed into DMSO-d_6 and took the 1H NMR test as shown in Fig. S10. The high peak at 3.47 ppm is attributed to H_2O that sneaked into the electrode plate unavoidably from the air during the process of disassembling battery.
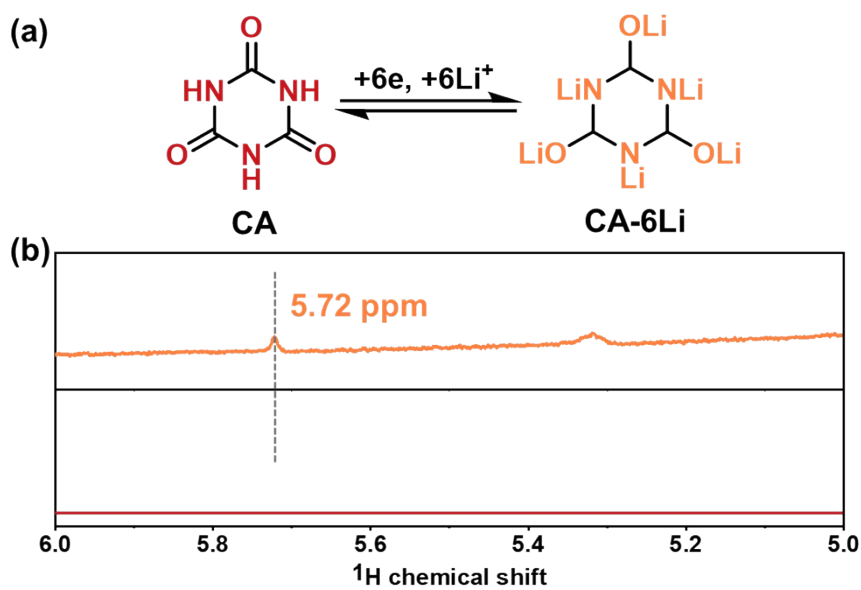
Figure S11. Corresponding ^{1}H NMR spectra for pure CA (red) and exsolution object (orange) of the CA cathode after discharge by DMSO-d_6.
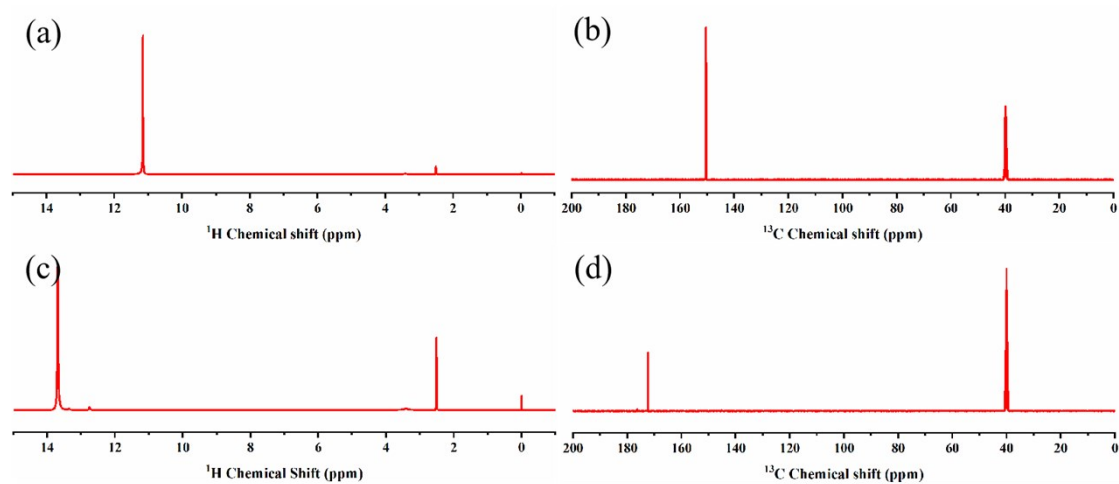
Figure S12. (a, b) ^{1}H and ^{13}C NMR spectras of CA, (c, d) ^{1}H and ^{13}C NMR spectras of TTCA.

Table S1. Representative example of organic cathode materials for lithium batteries.

Redox center	Represent structures	$C_{theoretical}$ (mAh g^{-1}), transfer X mol Li$^+$ per unit	Current density (mA g^{-1})	$C_{measured}$ (mAh g^{-1})	Capacity decay rate, cycles
	 This work	908, 6	2000	820.6	0.26% per cycle, 200
	 TTA[8]	471, 4	30	422	1.16% per cycle, 44
	 Poly-C$_6$S$_6$[9]	609, 6	60.9	150	NA, 200
	 DMTS[10]	849, 4	84.9	720	0.36% per cycle, 50
	 S$_x$ (3 ≤ x ≤ 8)[11]	425.4 (X=3), 4	425.4	388.4	0.025% per cycle, 1200
	 C$_6$O$_6$[12]	957, 6	50	~750	0.18% per cycle, 100
	 PTO[13]	409, 4	NA	360	0.89% per cycle, 50
	 AQ[14]	257, 2	300	222	1.13% per cycle, 50
	 ND H[15]	222, 4	111	170	0.55 per cycle, 100
		319, 2	20	249	0.2% per cycle, 100
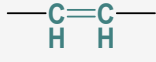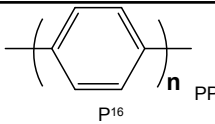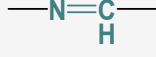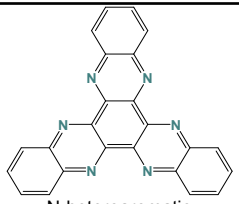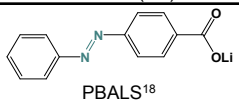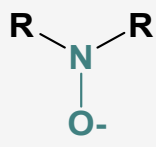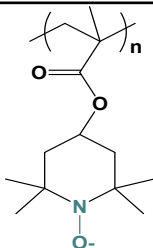
	PDB[7a]				
$-\overset{H}{\underset{H}{C}}=\overset{H}{\underset{H}{C}}-$	P[16] (PP)	353, 1	40	~80	0.25% per cycle, 100
$-N=\overset{H}{C}-$	N-heteroaromatic triquinoxalinylene molecules (3Q)[17]	400, 6	800	395	0.17% per cycle, 200
$-N=N-$	PBALS[18]	203, 2	101.5	220	0.19% per cycle, 100
R∖N∕R ⎥ O-	PTMA[19]	111, 2	111	109	0.055% per cycle, 200

Table S2. Corresponding theoretical capacities of organic materials combined with n lithiums respectively.
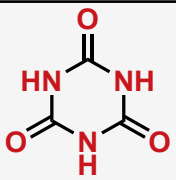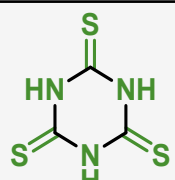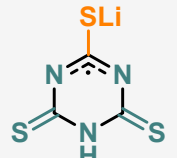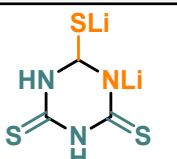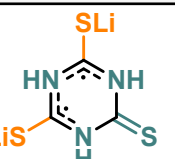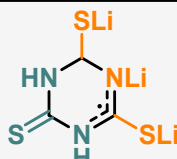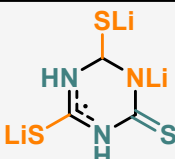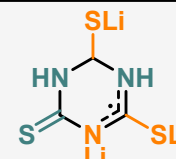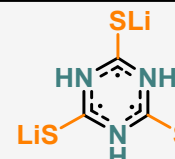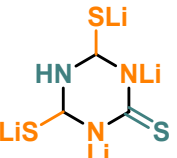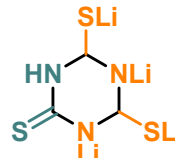
nLi		
2Li	422	306
4Li	844	612
6Li	1246	918

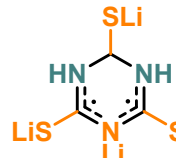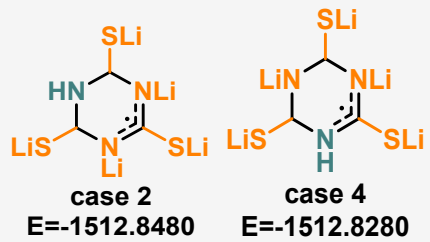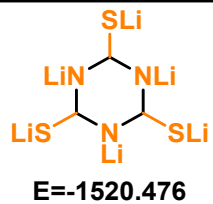**Table S3.** All possible molecular structures of Li_nTTCA (n=1, 2, 3, 4, 5, 6) based on DFT calculations. Unit of energy (E): hartree.

5Li

case 2
E=-1512.8480

case 4
E=-1512.8280

6Li

E=-1520.476

15

References

1   K. Hernandez-Burgos, S. E. Burkhardt, G. G. Rodríguez-Calero, R. G. Hennig, H. D. Abruna, *J. Phys. Chem. C,* 2014, **118**, 6046-6051.

2   G. Kresse, J. Hafner, *Phys. Rev. B,* 1993, **48**: 13115-13118.

3   G. Kresse, J. Furthmüller, *Phys. Rev. B,* 1996, **54**: 11169-11186.

4   G. Kresse, J. Furthmüller, *Comput. Mater. Sci.,* 1996, **6**: 15-50.

5   JP. Perdew, K. M. Burke, *Phys. Rev. Lett.,* 1996, **77**: 3865-3868.

6   PE. Blöchl, *Phys. Rev. B,* 1994, **50**: 17953-17979.

7   (a) J. Xie, Z. L. Wang, Z. C. J. Xu, Q. C. Zhang, *Adv. Energy Mater.,* 2018, **8**, 1703509; (b) S. Schmidt, D. Sheptyakov, J.-C. Jumas, M. Medarde, P. Benedek, P. Novák, S. Sallard, C. Villevieille, *Chem. Mat.,* 2015, **27**, 7889-7895; (c) K. W. Nam, S. S. Park, R. Dos Reis, V. P. Dravid, H. Kim, C. A. Mirkin, J. F. Stoddart, *Nat. Commun.,* 2019, **10**, 1-10.

8   S.-R. Deng, L.-B. Kong, G.-Q. Hu, T. Wu, D. Li, Y.-H. Zhou, Z.-Y. Li, *Electrochim. Acta,* 2006, **51**, 2589-2593.

9   M. B. Preefer, B. Oschmann, C. J. Hawker, R. Seshadri, F. Wudl, *Angew. Chem.,* 2017, **129**, 15314-15318.

10 M. Wu, Y. Cui, A. Bhargav, Y. Losovyj, A. Siegel, M. Agarwal, Y. Ma, Y. Z. Fu, *Angew. Chem. Int. Edit.,* 2016, **55**, 10027-10031.

11 D. Y. Wang, Y. Si, W. Guo, Y. Fu, *Adv. Sci.* 2020, **7**, 1902646.

12 Y. Lu, X. Hou, L. Miao, L. Li, R. Shi, L. Liu, J. Chen, *Angew. Chem. Int. Edit.,* 2019, **58**, 7020-7024.

13 Y. Liang, P. Zhang, J. Chen, *Chem. Sci.,* 2013, **4**, 1330-1337.

14 Z. Lei, W. Wei-kun, W. An-bang, Y. Zhong-bao, C. Shi, Y. Yu-sheng, *J. Electrochem. Soc.,* 2011, **158**, A991-A996.

15 D. J. Kim, S. H. Je, S. Sampath, J. W. Choi, A. Coskun, *RSC Adv.,* 2012, **2**, 7968-7970.

16 L. Zhu, A. Lei, Y. Cao, X. Ai, H. Yang, *Chem. Commun.,* 2013, **49**, 567-569.

17 C. Peng, G.-H. Ning, J. Su, G. Zhong, W. Tang, B. Tian, C. Su, D. Yu, L. Zu, J. Yang, *Nat. Energy,* 2017, **2**, 1-9.

18 C. Luo, X. Ji, S. Hou, N. Eidson, X. L. Fan, Y. J. Liang, T. Deng, J. J. Jiang, C. S. Wang, *Adv. Mater.,* 2018, **30**, 9.

19 J.-K. Kim, G. Cheruvally, J.-H. Ahn, Y.-G. Seo, D. S. Choi, S.-H. Lee, C. E. Song, *J. Ind. Eng. Chem.,* 2008, **14**, 371-376.